


# Cholesterol biogenesis is a PTEN-dependent actionable node for the treatment of endocrine therapy-refractory cancers

Irmak Kaysudu<sup>1</sup> | Taha Bugra Gungul<sup>1</sup> | Sena Atici<sup>1</sup> | Sevval Yilmaz<sup>1</sup> | Engin Bayram<sup>2</sup> | Gozde Guven<sup>3</sup> | Nihal Terzi Cizmecioglu<sup>3</sup> | Ozgur Sahin<sup>4</sup> | Gurkan Yesiloz<sup>5</sup> | Berat Zeki Haznedaroglu<sup>2</sup> | Onur Cizmecioglu<sup>1,6</sup> 

<sup>1</sup>Department of Molecular Biology and Genetics, Bilkent University, Ankara, Turkey

<sup>2</sup>Institute of Environmental Sciences, Bogazici University, Istanbul, Turkey

<sup>3</sup>Department of Biological Sciences, Middle East Technical University, Ankara, Turkey

<sup>4</sup>Department of Biochemistry and Molecular Biology, Hollings Cancer Center, MUSC, Charleston, South Carolina, USA

<sup>5</sup>Institute of Materials Science and Nanotechnology, Bilkent University, Ankara, Turkey

<sup>6</sup>Department of Molecular Biology and Genetics, Faculty of Science, Bilkent University, Ankara, Turkey

## Correspondence

Onur Cizmecioglu, Department of Molecular Biology and Genetics, Faculty of Science, SB-310, Bilkent University, Ankara 06800, Turkey.  
Email: [onur.cizmecioglu@bilkent.edu.tr](mailto:onur.cizmecioglu@bilkent.edu.tr)

## Funding information

Türkiye Bilimsel ve Teknolojik Araştırma Kurumu, Grant/Award Number: 118Z976

## Abstract

PTEN and PIK3CA mutations are the most prevalent PI3K pathway alterations in prostate, breast, colorectal, and endometrial cancers. p110 $\beta$  becomes the prominent PI3K isoform upon PTEN loss. In this study, we aimed to understand the molecular mechanisms of PI3K dependence in the absence of PTEN. Using online bioinformatical tools, we examined two publicly available microarray datasets with aberrant PI3K activation. We found that the rate-limiting enzyme of cholesterol biogenesis, SQLE, was significantly upregulated in p110 $\beta$ -hyperactivated or PTEN-deficient mouse prostate tumors. Concomitantly, the expression of cholesterol biosynthesis pathway enzymes was directly correlated with PI3K activation status in microarray datasets and diminished upon PTEN re-expression in PTEN-null prostate cancer cells. Particularly, PTEN re-expression decreased SQLE protein levels in PTEN-deficient prostate cancer cells. We performed targeted metabolomics and detected reduced levels of cholesteryl esters as well as free cholesterol upon PTEN re-expression. Notably, PTEN-null prostate and breast cancer cell lines were more sensitive to pharmacological intervention with the cholesterol pathway than PTEN-replete cancer cells. Since steroid hormones use sterols as structural precursors, we studied whether cholesterol biosynthesis may be a metabolic vulnerability that enhances antihormone therapy in PTEN-null castration-resistant prostate cancer cells. Coinhibition of cholesterol biosynthesis and the androgen receptor enhanced their sensitivity. Moreover, PTEN suppression in endocrine therapy-resistant luminal-A breast cancer cells leads to an increase in SQLE expression and a corresponding sensitization to the inhibition of cholesterol synthesis. According to our data, targeting cholesterol biosynthesis in combination with the

**Abbreviations:** CDI, coefficient of drug interaction; DAVID database, Database for Annotation, Visualization and Integrated Discovery; DMSO, dimethylsulfoxide; ENTPD5, ectonucleoside triphosphate diphosphohydrolase 5; GEO, Gene Expression Omnibus; HMGCR, 3-hydroxy-3-methylglutaryl-CoA reductase; KEGG, Kyoto Encyclopedia of Genes and Genomes; KM plotter, Kaplan–Meier plotter; PH domain, Pleckstrin homology domain; PI, phosphatidylinositol; PI3K, phosphoinositide 3-kinase; PIP2, phosphatidylinositol bisphosphate; PIP3, phosphatidylinositol trisphosphate; PTEN, phosphatase and tensin homolog deleted on chromosome 10; SQLE, squalene epoxidase; SREBP1C, sterol-regulatory element-binding protein 1C.

Irmak Kaysudu, Taha Bugra Gungul, and Sena Atici contributed equally to this work.

This is an open access article under the terms of the [Creative Commons Attribution-NonCommercial](https://creativecommons.org/licenses/by-nc/4.0/) License, which permits use, distribution and reproduction in any medium, provided the original work is properly cited and is not used for commercial purposes.

© 2023 The Authors. *Cancer Science* published by John Wiley & Sons Australia, Ltd on behalf of Japanese Cancer Association.

hormone receptor signaling axis can potentially treat hormone-resistant prostate and breast cancers.

**KEYWORDS**

carcinogenesis, cholesterol biosynthesis, PI3K, PTEN-null, signal transduction

## 1 | INTRODUCTION

PI3K pathway is crucial for proliferation, cellular metabolism, and response to growth factors. PI3K acts as a lipid kinase and catalyzes the phosphorylation of PI lipids at the 3'OH group. Phosphorylated PIs recruit PH domain-containing proteins to the plasma membrane and activate downstream signaling components. PTEN is a dual lipid and protein phosphatase. PTEN dephosphorylates PI3K-produced PIP3 back into PIP2. Homozygous deletions and mutations of PTEN are highly common in carcinogenesis. PTEN loss causes overactivation of the PI3K pathway, and cancer cells become primarily dependent on the p110 $\beta$  isoform.<sup>1</sup>

The PI3K pathway modulates metabolic processes like lipid biosynthesis and nutrient transport and regulates metabolic transcription factors. The PI3K pathway activates the key lipogenic transcription factor SREBP1C through inhibition of GSK3.<sup>2</sup> PTEN loss, on the other hand, causes adipogenic-like transformation in hepatocytes and upregulates the transcription of genes related to lipogenesis and  $\beta$ -oxidation through PPAR $\gamma$  and SREBP1. PI3K activation induced by PTEN loss promotes protein glycosylation and folding through ectonucleoside triphosphate ENTPD5, increases ATP consumption, and promotes the Warburg effect.<sup>3</sup> Thus, although dietary restriction can lower the activity of the PI3K pathway, tumors that harbor PTEN loss or PI3K mutations can resist its beneficial effects.<sup>4</sup> On the other hand, the systemic increase in PTEN in normal cells has been shown to lead to a decrease in glucose and glutamine utilization, an increase in oxidative phosphorylation, and resistance to oncogenic transformation in vivo.<sup>5</sup> Along these lines, recent work has shown that lipid raft activation is dependent on cholesterol production in PTEN-null breast and prostate cancer cell lines.<sup>6</sup>

For a variety of reasons, cancer cells have an increased demand for cholesterol. Cholesterol is a precursor of the steroid hormones and a crucial component of the cell membrane. Synthesis of cholesterol begins with mevalonate production from acetate.<sup>7</sup> In this pathway, HMGCR and SQLE are two rate-limiting enzymes, and statins are widely used as cholesterol-lowering agents worldwide by targeting HMGCR. Squalene is the substrate for the SQLE enzyme, which introduces an epoxide group to squalene, producing 2,3 epoxysqualene. The development and proliferation of hormone-dependent cancer cells require steroid hormones. Statin-using patients with hormone-dependent cancers were reported to have a reduced mortality rate.<sup>8</sup> Besides, SQLE-targeting agents were proposed as a new treatment option for cancer.<sup>9</sup>

In our study, we aimed at understanding the molecular mechanisms for Class IA PI3K isoform prominence, PTEN loss-induced metabolic rewiring, and biomarker potential of SQLE in hormone-dependent

prostate and breast carcinogenesis. We used regulated expression of PTEN in PTEN-null prostate cancers and performed targeted metabolomics to identify changes in the cholesterol synthesis pathway. Our results implicate a PTEN loss-dependent upregulation of cholesterol synthesis in hormone-dependent breast and prostate cancers, and we hypothesize that metabolic targeting of this pathway has the potential to treat antihormone therapy-resistant breast and prostate cancers.

## 2 | MATERIALS AND METHODS

### 2.1 | Cell culture

MCF7, T47D, tamoxifen-resistant MCF7, tamoxifen-resistant T47D,<sup>10</sup> or tamoxifen-resistant T47D-shPTEN2 cells were cultured in phenol red-free DMEM (Gibco) supplemented with 8% FBS (Capricorn), 1% penicillin-streptomycin (Gibco), 1% L-glutamine (PAN-Biotech), and 4  $\mu$ g/mL insulin (Merck). HEK293, mouse embryonic fibroblast (MEF), Cama-1, and DU145 were cultured in DMEM (Biowest), with 8% FBS and 1% penicillin-streptomycin. BT549, ZR-75-1, PC3, LNCaP, and C4-2 cell lines were cultured in RPMI-1640 (Biowest) supplemented with 8% FBS and 1% penicillin-streptomycin. The cells were maintained at 37°C and in a humidified atmosphere with 5% CO<sub>2</sub> conditions and were regularly tested for mycoplasma and STR profiling.

### 2.2 | Plasmid transfection and generation of stable cell lines

For the generation of the Tet-on system, rtTA plasmid (Clontech) and pRXTN (Addgene Cat#47916) or pRXTN-PTEN-WT were cotransduced to PC3, LNCaP, or C4-2 cell lines. HEK293 cells were cotransfected with the plasmid of interest and retroviral packaging plasmids pCMV-VSV-G (Addgene Cat#8454) and gag/pol (Addgene Cat#14887) by using Lipofectamine 3000 (Thermo) according to the manufacturer's protocol. The antibiotic selections were conducted with 400  $\mu$ g/mL geneticin (Gibco) and nourseothricin (Jena Biosciences).

Two different shRNA constructs were used to deplete PTEN expression in tamoxifen-resistant T47D cell lines (shPTEN1: CCGGCCTAGAACTTATCAAACCCTTCTCGA GAAGGGTTTGATAAGTTCTA GCTTTT, shPTEN2: CCGGCGACTTAGACTTGACCTAT ATCTCGAG ATATAGGTCAAGTCTAAGTCGTTTTT). The antibiotic selection was conducted with 2  $\mu$ g/mL puromycin (Gibco).

## 2.3 | Immunoblotting

Standard protocols were followed for immunoblot analyses.<sup>11,12</sup> The membranes were developed by Pierce ECL (Thermo) on Amersham Imager 600. SREBP2 antibody is from Santa Cruz (SC-271616). The remainder of the antibodies are from Cell Signaling; catalogue numbers are available upon request.

## 2.4 | RT-qPCR

RNA isolation was performed by using the RNeasy Plus Mini Kit (Qiagen). A total of 1000 ng of RNA was converted into cDNA by the BioRad iScript cDNA Synthesis Kit (Bio-Rad) according to the manufacturer's protocol. Then, 50 ng cDNA was conducted to qPCR with SsoAdvanced Universal Inhibitor-Tolerant SYBR Green Supermix (Bio-Rad) according to the manufacturer's protocol on Roche Light Cycler Real-Time PCR. GAPDH was used as an internal control. mRNA fold change analysis was performed by the  $2^{-\Delta\Delta CT}$  method. Primer sequence information is available upon request.

## 2.5 | In silico analyses

GSE21543 and GSE46799 microarray datasets were stored at the GEO database. The GSE21543 dataset contains expression levels for p110 $\beta$ -driven mouse prostatic intraepithelial neoplasia (mPIN). GSE46799 contains microarray data of PTEN loss-induced prostate carcinogenesis in mice. Datasets were analyzed with GEO2R by using Benjamini-Hochberg 0.05 cutoff value. Gene set enrichment analyses were performed through the DAVID website<sup>13,14</sup> with KEGG pathway results for both datasets. Significantly upregulated genes were selected according to the threshold 0.05.

SQLI copy number alterations and survival rates for prostate and breast cancer were retrieved from cBioPortal.<sup>15,16</sup> The biomarker potential of the *SQLI* gene was assessed with chemotherapy-treated breast cancer patient data on the ROC plotter<sup>17</sup> and KM plotter.<sup>18</sup> Relapse-free survival at 5 years of tamoxifen endocrine therapy-treated breast cancer patient data was used.

## 2.6 | Statistical analysis

GraphPad Prism 9.2 was used for statistical analysis and for the determination of IC50 concentrations of the drugs. The significant differences in the experimental groups were calculated by two-tailed Student's *t*-test, and multiple comparisons were done with one-way ANOVA.

The quantification of the band intensities of Western blot data was performed with ImageJ. The coefficient of drug interaction (CDI) values of combination treatments were calculated according to the following formula:

$$CDI = \frac{\text{survival \% (drugA + drugB)}}{\text{survival \% (drugA)} \times \text{survival \% (drugB)}}$$

Extended experimental procedures are available as supplemental information (Data S1).

## 3 | RESULTS

Disease models indicated that overexpression of p110 $\beta$  leads to prostatic intraepithelial neoplasia (PIN) formation in prostate tissue, which is considered the first step in malignant transformation, when ducts and acini of the prostate begin to fill with cells. Sequencing of human patient samples identified  $\beta$ -1051K mutation as a gain-of-function mutation in the *PIK3CB* gene in metastatic prostate cancer.<sup>19</sup> However, cellular mechanisms leading the way to p110 $\beta$  dependence remain incompletely understood.

In order to gain insight into the mechanisms determining PI3K isoform prevalence, we evaluated the GEO datasets GSE21543 and GSE46799. GSE21543 contains data from wild-type and transgenic p110 $\beta$  mice, where myristoylated p110 $\beta$  was expressed in prostate tissue via an N-terminal myristoylation tag for the *PIK3CB* gene. The myristoylation tag activates p110 $\beta$  constitutively, resulting in PIN formation. The GSE46799 dataset consists of wild-type and PTEN-floxed mice. PTEN depletion in mouse prostate tissue constitutively activates the PI3K pathway. In both datasets, upregulated genes were analyzed in GEO2R and DAVID v6.8.<sup>14</sup> KEGG pathway results from DAVID database analyses of significantly upregulated pathways were primarily metabolic pathways, for example, glycolysis, steroid biosynthesis, and carbon metabolism (Figure 1A).

Within the metabolic pathways, the most promising ones were selected as transcriptional regulation, cholesterol synthesis, and metabolism of energy after applying a *p*-value cutoff of <0.05. Significantly upregulated candidate genes that were selected from metabolic pathway-related genes were *CREB3L4*, *AK4*, and *SQLI* upon constitutive PI3K activation (Figure 1B).

Since PTEN loss leads to p110 $\beta$  prominence in cancer, we aimed to corroborate the GSE21543 and GSE46799 dataset analyses by quantifying mRNA levels of candidate genes with qPCR in an activated p110 $\beta$ -expressing MEF system. Cellular proliferation of MEFs becomes contingent upon the activated isoform, which allowed us to repress PI3K pathway activity by the p110 $\beta$ -specific inhibitor KIN-193. Upon PI3K pathway inhibition, the mRNA levels of both the *SQLI* and *AK4* genes, but not that of *CREB3L4*, were decreased (Figure 1C and Figure S1A). These results suggest that *SQLI* and *AK4* expression levels are regulated by the activated PI3K pathway. Since *AK4* does not have any kinase activity, it is not a directly actionable target. Moreover, regulation of cellular levels of cholesterol can have implications for the effectiveness of the PI3K pathway, and *SQLI* might be a downstream target of the PI3K pathway critical for selective isoform predominance. Therefore, we rather focused on the *SQLI* gene for further analysis.

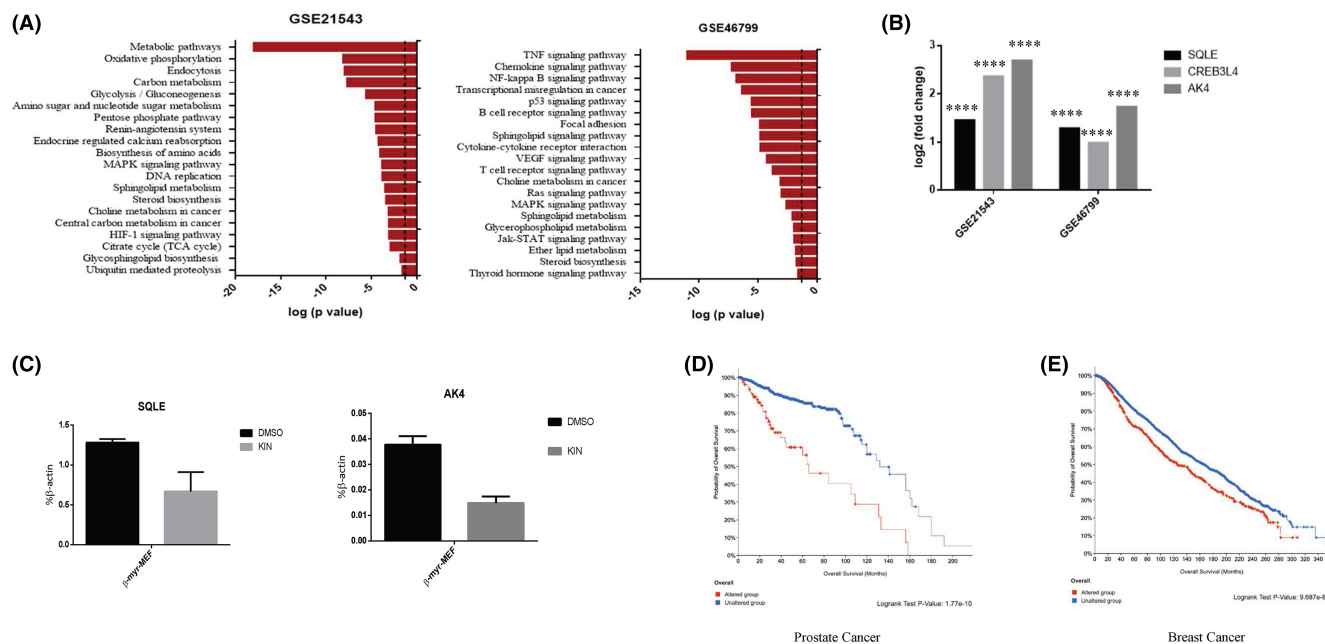


**FIGURE 1** Metabolic pathways are altered upon deregulated phosphoinositide 3-kinase (PI3K) signaling in cancer. (A) GSE21543 and GSE46799 microarray datasets were analyzed in DAVID v6.8 for Kyoto Encyclopedia of Genes and Genomes (KEGG) pathway enrichment analysis ( $p < 0.05$ ). (B) Logarithmic fold changes (logfc) of candidate genes between normal and PI3K pathway-upregulated samples were analyzed in the same datasets ( $****p < 0.005$ ). (C) mRNA levels were quantified in activated PIK3CB expressing MEFs upon inhibitor treatment. Levels are normalized against Actin. (D) Prostate cancer patients have lower survival rates in the squalene epoxidase (SQLE)-altered group (altered group  $n = 114$ , unaltered group  $n = 1359$ ). (E) Breast cancer patients have significant decrease in survival rate in the SQLE-altered group (altered group  $n = 1057$ , unaltered group  $n = 6486$ ).

### 3.1 | In silico analyses of cholesterol synthesis pathway genes upon PI3K pathway activation

To determine the potential involvement of the SQLE gene in tumorigenesis, in silico analyses were performed on hormone-dependent cancers like prostate, breast, colon, and ovarian cancer, which exhibit high alteration frequency for SQLE (Figure S1B). In several advanced-stage breast and prostate cancer datasets, we have observed alteration frequencies between 20% and 30% for the SQLE gene. Furthermore, the amplification rate of SQLE in breast cancer is approximately 17% and 15% for invasive breast carcinoma (Figure S1B).

To test if the expression level of SQLE is correlated with patient survival, we analyzed prostate and breast cancer datasets and showed that patients with SQLE amplification have a significantly lower survival compared with the unaltered patient group ( $p$ -values of  $1.77e^{-10}$ , prostate and  $9.687e^{-6}$ , breast; Figure 1D,E).

We then wanted to find out if SQLE is the sole target of PI3K in the cholesterol synthesis pathway. For the GSE21543 dataset, apart from the MVD gene, all cholesterol synthesis pathway genes appear to be significantly upregulated in p110 $\beta$  myristoylated samples (Figure S1C). Likewise, cholesterol pathway enzymes appear to be upregulated in PTEN-floxed prostate samples in the GSE46799 dataset (Figure S1D).

To elucidate whether cholesterol synthesis pathway genes are regulated upon short-term PTEN re-expression in a PTEN-null

background, we generated a PTEN inducible PC3 model by transduction of pRXTN-PTEN-wt expression vector. Upon PTEN re-expression in PC3s, the mRNA levels of HMGCS, HMGCR, PMVK, MVD, FDPS, and SQLE were downregulated (Figure 2A). According to these analyses, PTEN re-expression inversely correlated with cholesterol pathway enzymes, implicating a regulatory function of PI3K in cholesterol synthesis.

To analyze the impact of PTEN expression on protein levels of cholesterol pathway components, we established LNCaP and C4-2 models by stable transfection with pRXTN-PTEN-wt vector. PTEN re-expression in all models led to a significant downregulation of SQLE levels alongside the expected reduction in p-AKT, while HMGCS levels were modestly reduced in PC3 and C4-2 cells (Figure 2B, for unprocessed original scans; Figure S2). Our findings suggest that PTEN status and PI3K activity govern cholesterol biosynthesis, mainly at the level of SQLE.

### 3.2 | Differential sensitivities to cholesterol synthesis inhibitors based on PTEN status

To analyze the effects of PTEN on cholesterol pathway and viability of cells, pharmacological inhibitors targeting the rate-limiting enzymes of the pathway were used. Simvastatin and terbinafine are available as FDA approved pharmacologic inhibitors for the first and second rate-limiting enzymes, HMGCR and SQLE, respectively.<sup>20</sup>

To investigate the correlation of PTEN and cholesterol synthesis, cholesterol pathway inhibitors were used in PTEN-wt and PTEN-null cancer cells. Firstly, PTEN-null PC3 and PTEN-wt DU145 cell lines were treated with either simvastatin or terbinafine. PC3 cells were more sensitive to cholesterol synthesis inhibition by simvastatin and terbinafine in terms of viability (Figure 3A). Breast cancer cell lines exhibited a similar sensitivity profile based on their PTEN expression status. BT549, a PTEN-null cell line, was sensitive to simvastatin

treatment at high doses. PTEN-wt MCF7 cells were more resistant to SQLE inhibition compared with BT549 cells (Figure 3B). Our results demonstrated that PTEN-null cell lines were inherently more sensitive to inhibitors of the cholesterol synthesis pathway than PTEN-replete cell lines.

Biochemical analyses were performed for the identification of possible links between the cholesterol pathway and PTEN status. PC3 and DU145 cells were treated with DMSO, simvastatin,

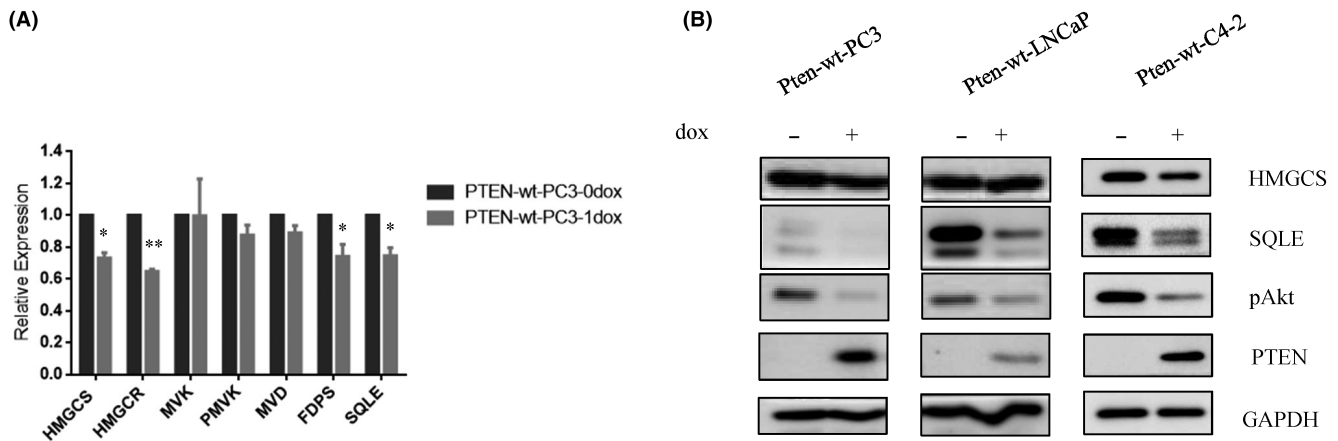


**FIGURE 2** Cholesterol pathway gene expression is regulated by phosphoinositide 3-kinase (PI3K) signaling. (A) mRNA levels of cholesterol synthesis pathway genes were quantified in doxycycline-induced PC3 cells (\* $p < 0.05$ ; \*\* $p < 0.01$ ; \*\*\* $p < 0.005$ ; \*\*\*\* $p < 0.0001$ ). (B) Prostate cancer cell lines were treated with doxycycline for 3 days. HMGCS, SQLE, pAKT S473, and PTEN expression levels were detected by immunoblotting. GAPDH was used as loading control.

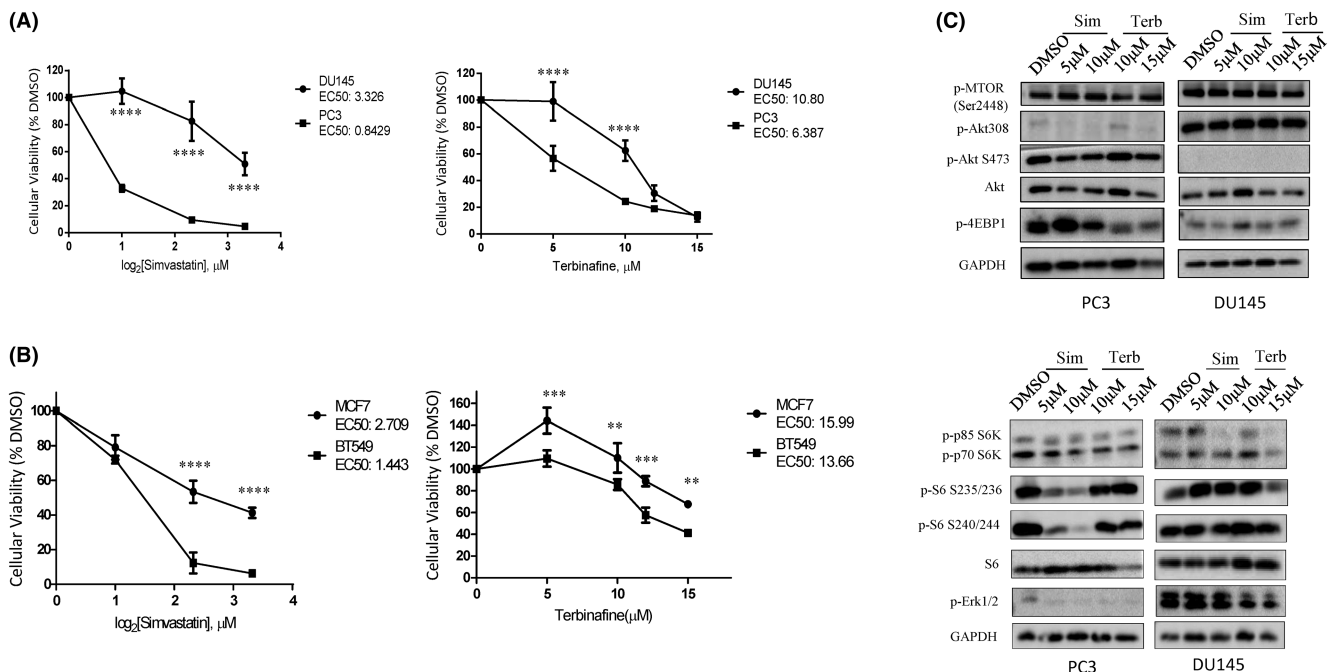


**FIGURE 3** PTEN levels affect cholesterol pathway inhibitor sensitivity in prostate and breast cancer cells. (A) Proliferation of PTEN-wt DU145 and PTEN-null PC3 prostate cancer cells were quantified upon simvastatin and terbinafine treatment. (B) Cellular viability was assessed for PTEN-wt MCF7 and PTEN-null BT549 breast cancer cell lines \*\* $p < 0.01$ ; \*\*\* $p < 0.005$ ; \*\*\*\* $p < 0.0001$  (error bars depict standard deviations,  $n = 3$ ). (C) Different concentrations of terbinafine and simvastatin were administered to PTEN-null PC3 and PTEN-wt DU145 cells. Immunoblots with the depicted antibodies were shown for PC3 on the left and DU145 on the right.

and terbinafine for 2 days. Phosphorylation levels of several PI3K pathway components were quantified with immunoblots. Phosphorylation of AKT at T308 and S473 was decreased in PC3 upon treatment with higher doses of simvastatin and terbinafine, whereas no difference was observed in DU145s (Figure 3C, upper panel). There was no change in mTOR phosphorylation between PC3 and DU145, nor was there a change upon inhibitor treatment. 4EBP1 phosphorylation at S65 was in line with p-Akt levels. We observed a significant decrease in p-4EBP1 in PC3 upon treatment with high doses of the inhibitors, but there was no change in DU145. Along these lines, phosphorylation of S6 is affected by PTEN status and cholesterol synthesis inhibitors. While the phosphorylation of S6 was unchanged in DU145 in both the terbinafine and simvastatin treatments, S6 phosphorylation of crucial residues was decreased upon simvastatin treatment in PC3s (Figure 3C, for unprocessed original scans; Figure S2).

These findings suggest that PTEN status influences susceptibility to cholesterol pathway inhibition, presumably via the PI3K-AKT-4EBP1 axis. This implicates a possible involvement of cholesterol biogenesis in growth factor signaling.

### 3.3 | Metabolomics of PTEN-inducible prostate cancer cells and biomarker potential of the cholesterol pathway

To test the impact of PTEN on cholesterol-based metabolite levels, we used our PTEN-inducible C4-2 cellular models and performed a mass spectrometry-based metabolomics using a targeted metabolomics kit.<sup>21</sup> In addition to wild-type PTEN (PTEN-wt), we have established a lipid- (G129E) or protein phosphatase-deficient (Y138L) PTEN alongside a catalytic dead mutant (C124S). There was a significant increase in PTEN expression upon induction with doxycycline in all cell lines, with a concomitant decrease in p-AKT only when the lipid phosphatase-proficient PTEN was expressed (Figure S3A). Flow injection analysis–mass spectrophotometry revealed quantifications of certain cholesterol esters upon PTEN-wt and mutant PTEN expressions. Levels of two cholesteryl esters, namely CE (22:5) and CE (22:6) were significantly downregulated (FC>1.5 and  $p < 0.05$ ) upon PTEN-wt and Y138L-PTEN expression compared with empty vector, whereas G129E-PTEN and C124S-PTEN expressions had no effect (Figure 4A and Table S1) This suggests that the lipid phosphatase

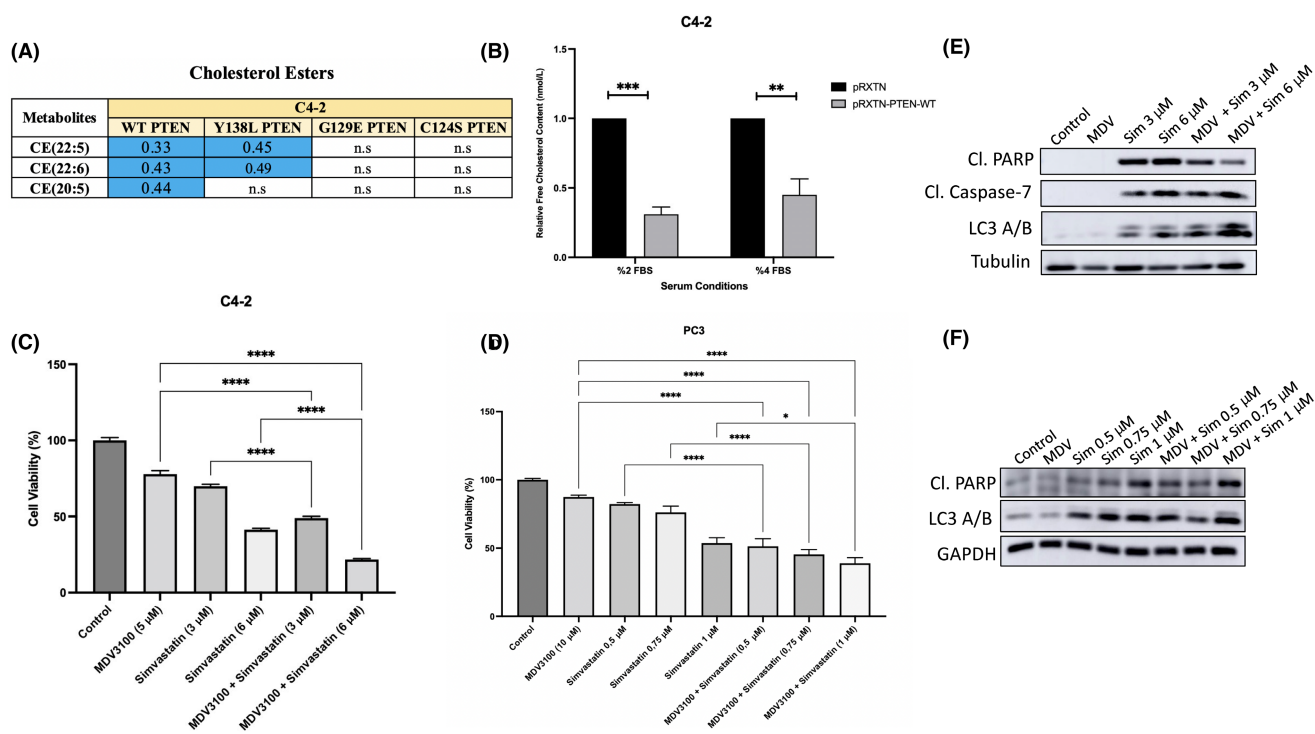


**FIGURE 4** Targeted metabolomics reveal regulation of cholesterol levels by PTEN in prostate cancer. (A) Quantifications of targeted metabolomics data for selected cholesterol esters. The table depicts changes of C4-2 cells for each PTEN variant and fold change (FC) values relative to empty vector metabolite levels. Blue boxes represent the significant downregulation of metabolites (FC>1.5 and  $p < 0.05$ ) and nonsignificant (n.s) fold changes compared with control. Each sample has at least three biological replicates. (B) The free cholesterol content of dox-induced C4-2 cells incubated with 2% or 4% FBS was measured. Error bars show the SEM of three biological replicates (\*\* $p < 0.01$ ; \*\*\* $p < 0.001$ ). (C) Normalized viability of C4-2. Cells were treated with DMSO, 5 μM MDV3100, and 3 and 6 μM simvastatin alone or combined with MDV3100 for 5 days. (D) Normalized viability of PC3. Cells were treated with DMSO, 10 μM MDV3100, and 0.5, 0.75, or 1 μM simvastatin alone and combined with MDV3100 for 5 days. Error bars show the SEM of three biological replicates (\* $p < 0.05$ ; \*\* $p < 0.01$ ; \*\*\* $p < 0.001$ ; \*\*\*\* $p < 0.0001$ ). (E, F) The protein levels of cleaved PARP, cleaved caspase-7, and LC3 A/B were determined in either single- or combo-treated C4-2 (E) and PC3 (F) cells by immunoblotting. Tubulin and GAPDH were used as loading controls.

function of PTEN regulates cholesterol ester levels in prostate cancer cells. Since cholesterol esters are derived from free cholesterol, we also sought to determine whether PTEN expression affected the levels of free cholesterol. Thus, a free cholesterol assay was performed in low and intermediate serum conditions to quantify and compare the free cholesterol concentration of control and PTEN-wt-expressing cells. This assay revealed that PTEN expression significantly decreased the free cholesterol ( $p < 0.05$ ) compared with an empty vector (Figure 4B). Whereas the control cells exhibited 0.95 mmol/L of free cholesterol in both circumstances, PTEN-wt-expressing cells had 0.28 and 0.4 mmol/L of free cholesterol at 2% and 4% serum, respectively, representing a 70% and 48% reduction in their free cholesterol content.

The next step was to determine if the elevated cholesterol in PTEN-null prostate cancer cells represented a metabolic vulnerability that could be exploited in pharmacological inhibitor-based viability assays. We performed combination treatment of PTEN-null, CRPC cell lines PC3 and C4-2 with simvastatin, and the androgen receptor antagonist enzalutamide (MDV3100; Figure 4C,D). We observed moderate-to-high synergism (CDI values between 0.45 and 0.83) in both cell lines upon tandem treatment of cells with several doses of the drugs, implicating that castration resistance could be overcome by inhibiting cholesterol biosynthesis (Tables 1 and 2). We then sought to learn about the biochemical pathways leading to suppression of cell proliferation in combination treatment. Immunoblot analysis with C4-2 revealed enhanced PARP and caspase-7 cleavage in simvastatin- or combination-treated cells. There was a considerable increase in LC3 processing, indicating an upregulation in autophagy in addition to the apoptotic efflux in these cells (Figure 4E, for unprocessed original scans; Figure S2). PC3 exhibited similar alterations upon combination treatment, with an increase in PARP and LC3 cleavage implicating an increase in apoptotic and autophagic processes. (Figure 4F).

After demonstrating a rationale in 2D models of cellular growth, we tested the effect of combining simvastatin with enzalutamide in focus formation assays. Both C4-2 and PC3 displayed a synergistic response (CDI values between 0.36 and 0.63) to the combinatorial treatment of simvastatin and enzalutamide (Figure S4A,B and Tables 3 and 4). Next, we utilized soft agar growth assays, which closely correlates with tumorigenicity. In soft agar growth, simvastatin and enzalutamide combined treatment revealed a more substantial decrease in colony growth in two doses of the drug combinations. (Figure 5A and Figure S5A). Cancer spheroid microtissue models have enabled in recent years valuable information by more closely mimicking the 3D nature of tumors in situ.<sup>22</sup> In this context,

TABLE 1 Coefficient of drug interaction (CDI) values of MDV3100 (enzalutamide) and simvastatin on C4-2 viability.

Combination	CDI	Indication
MDV3100 5 $\mu$ M	0.80	Moderate synergism
Simvastatin 3 $\mu$ M	0.45	Synergism
Simvastatin 6 $\mu$ M		

TABLE 2 Coefficient of drug interaction (CDI) values of MDV3100 and simvastatin on PC3 viability.

Combination treatment	CDI	Indication
MDV3100 10 $\mu$ M	0.72	Moderate synergism
Simvastatin 0.5 $\mu$ M	0.68	Synergism
Simvastatin 1 $\mu$ M	0.83	Moderate synergism

TABLE 3 Coefficient of drug interaction (CDI) values of MDV3100 and simvastatin on C4-2 colony formation.

Combination	CDI	Indication
MDV3100 5 $\mu$ M	0.36	Synergism
Simvastatin 6 $\mu$ M		

TABLE 4 Coefficient of drug interaction (CDI) values of MDV3100 and simvastatin on PC3 colony formation.

Combination treatment	CDI	Indication
MDV3100	0.62	Synergism
Simvastatin 0.5 $\mu$ M	0.63	
Simvastatin 0.75 $\mu$ M	0.54	
Simvastatin 1 $\mu$ M		

we utilized 3D spheroids to understand the efficacy of our combinatorial inhibitors. Similar to soft agar growth, 3D spheroid growth of C4-2 was completely inhibited in simvastatin and enzalutamide-treated samples but not in cells treated with simvastatin or enzalutamide alone (Figure 5B and Figure S5B).

### 3.4 | Targeting cholesterol synthesis in luminal A type breast cancer cells upon PTEN loss

Our results implicated the importance of cholesterol production in cellular models of prostate carcinogenesis and in resistance to androgen deprivation therapies. The PI3K pathway appears to regulate the levels of several enzymes involved in cholesterol production, with SQLE being the most prominent. Since our results suggested that PTEN-deficient breast cancer cells may also be more susceptible to inhibition of cholesterol synthesis, we investigated a potential relationship between PTEN status and sensitivity to cholesterol biosynthesis in estrogen-dependent luminal A-type breast cancer cells in which PI3K activation is prevalent.

We analyzed levels of SQLE in various luminal A-type breast cancer cell lines which express PTEN to different levels. In addition, we used well-established MCF7 and T47D models of tamoxifen resistance (TamR).<sup>10</sup> Our results indicate that SQLE levels are lower in cell lines with high PTEN (Figure 6A, for unprocessed original scans; Figure S2). A second intriguing finding was that SQLE levels were elevated in tamoxifen-resistant MCF7 and T47D cells, whereas SREBP, which is the primary transcriptional regulator of the cholesterol production pathway,<sup>23</sup> did not change. Therefore, the PI3K

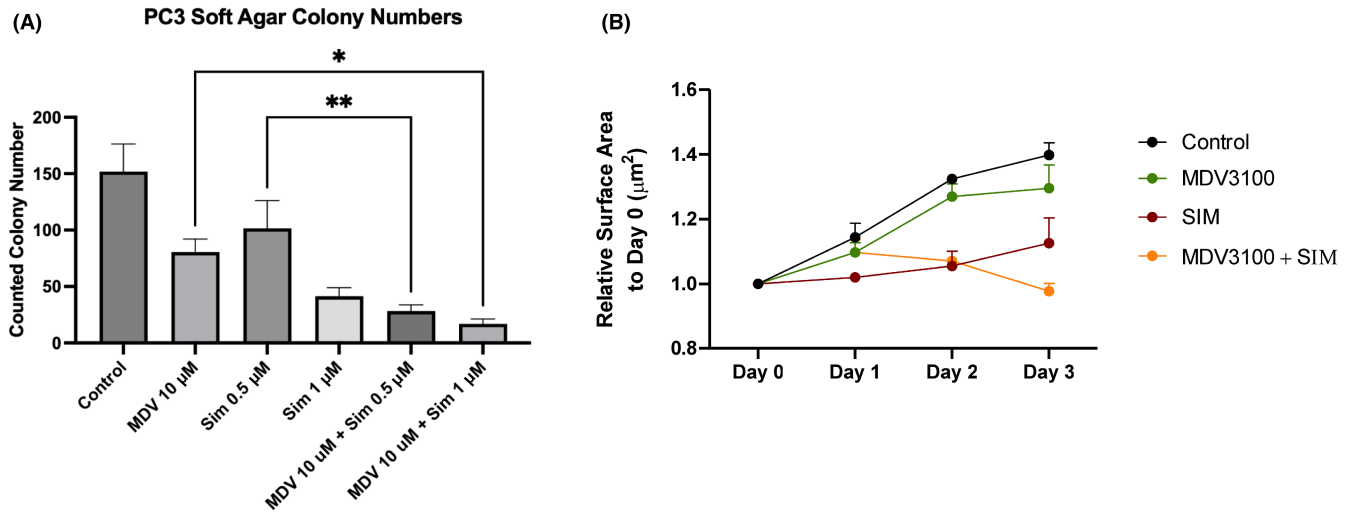


**FIGURE 5** MDV3100 and simvastatin combination treatment acted synergistically on PC3 and C4-2 in 3D growth models. (A) Number of PC3 colonies grown in soft agar after 15 days. Only the colonies that are larger than approximately 0.2mm in diameter were counted. Error bars depict the SEM of three biological replicates (\* $p < 0.05$ ; \*\* $p < 0.01$ ). (B) Analysis and monitoring of C4-2 under DMSO, MDV3100 alone, SIM alone, and combination of MDV3100+SIM ( $n = 3$ ). Spherically growing cells were monitored for 3 days, and relative surface areas were depicted.

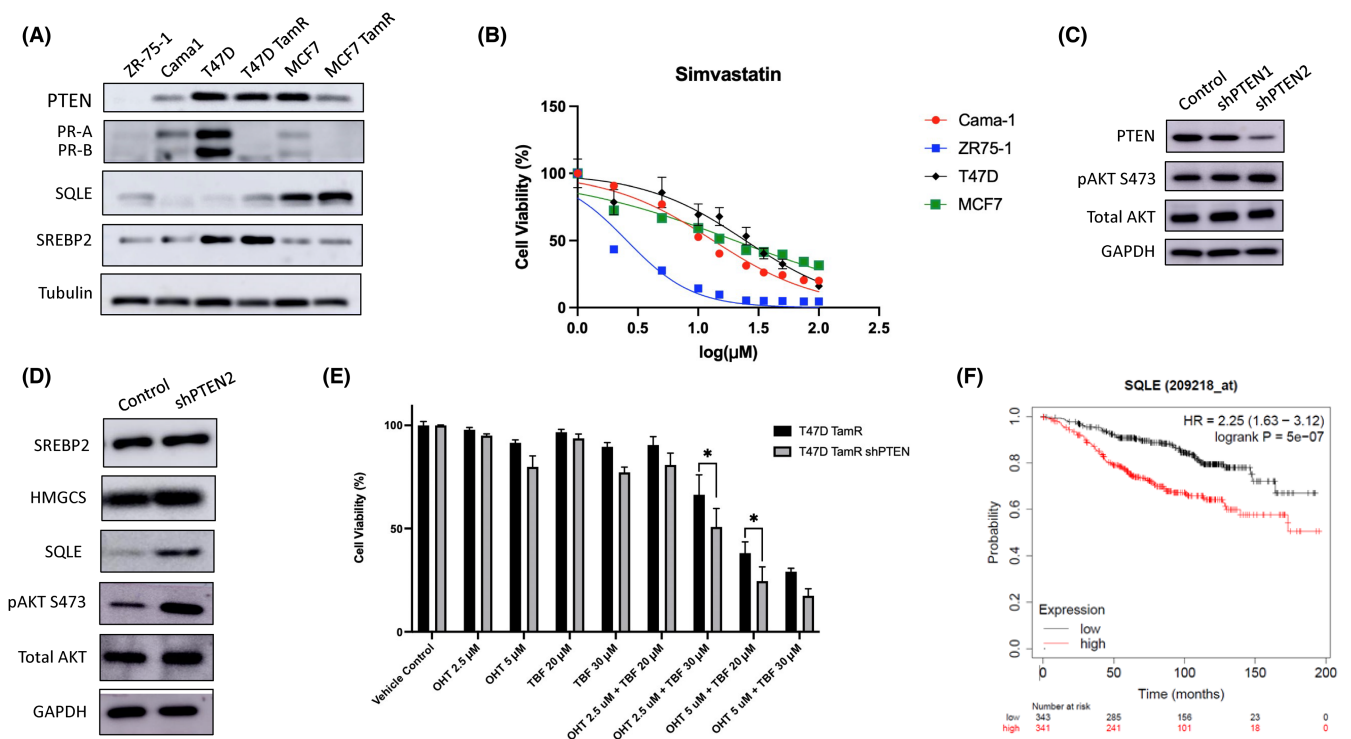


**FIGURE 6** PTEN status of luminal A-type breast cancer cell lines dictates the sensitivity to cholesterol metabolism inhibitors. (A) PTEN, progesterone receptor, SQLE, and SREBP2 expression levels were detected by immunoblotting. Tubulin was used as loading control. (B) Viabilities of Cama-1, ZR75-1, T47D, and MCF7 were determined by normalizing to control. Cells were treated with different concentrations of simvastatin for 5 days, and SRB assay was conducted. Error bars depict the SEM ( $n = 3$ ). (C) Immunoblot analysis of T47D-TamR cell lines after the transduction of lentiviral pLKO.1-puro-shPTEN plasmids. (D) Western blot analysis showing the rate-limiting enzymes of the cholesterol biosynthesis pathway in T47D-TamR and shPTEN T47D-TamR. (E) The viabilities of T47D-TamR and shPTEN T47D-TamR were normalized to control. The error bars show the SEM ( $n = 3$ , two-way ANOVA for multiple comparisons, \* $p < 0.05$ ). (F) The relapse-free survival of tamoxifen-treated ER+, HER2- breast cancer patients analyzed in terms of SQLE expression by KM plotter.



pathway appears to directly or indirectly affect the stability of SQLE protein as well as its transcriptional control. In addition, PTEN levels were a strong indicator of simvastatin sensitivity. In growth experiments, cells with the lowest amount of PTEN (e.g., ZR75-1) were the most sensitive to simvastatin (Figure 6B and Table 5). Next, we aimed to see the impact of acute changes in PTEN on SQLE levels as well as cellular sensitivity to cholesterol inhibition. To this end, we used shRNA vectors to downregulate PTEN in T47D-TamR. In addition to the anticipated upregulation of p-Akt, we found elevated levels of SQLE, while SREBP and HMGCS levels remained unchanged (Figure 6C,D, for unprocessed original scans; Figure S2). In cellular viability assays, we discovered that shPTEN T47D-TamR cells were more sensitive to the SQLE antagonist terbinafine than control cells (Figure S6A).

Upon PTEN knockdown, SQLE levels are consistently elevated at normal or low serum levels, eliminating a potential inadvertent effect of serum on SQLE (Figure S6B). We also determined an increased potency of tamoxifen and terbinafine combination for PTEN knockdown in certain drug combinations (Figure 6E and Table 6). These findings indicate the relevance of targeting cholesterol metabolism to effectively sensitize PTEN-low anti-hormone treatment-resistant breast tumors to tamoxifen.

Then, we evaluated the impact of SQLE on the survival of ER+/HER- breast cancer patients treated with endocrine therapy. In these datasets, a higher SQLE expression was associated with a 2.25-fold increase in the hazard ratio for mortality (Figure 6F). Lastly, we investigated the biomarker potential of SQLE in breast cancer patient cohorts treated with endocrine therapy. Using an ROC plotter, the 5-year relapse-free survival was analyzed based on their SQLE expression rate in response to tamoxifen. We found that SQLE expression is lower in patients (median expression: 1177 vs. 1643) responsive to tamoxifen treatment than in unresponsive individuals. The area under the curve for SQLE-sensitive samples is 0.639, with a  $p$ -value of  $5.2e^{-08}$ , indicating that SQLE could be a breast cancer biomarker with potential clinical utility (Figure S6C).

TABLE 5 PTEN mutation status of luminal A-type breast cancer cells and their half-maximal inhibitory concentrations (IC<sub>50</sub> values) for simvastatin treatment.

Cell line	PTEN mutation status	Simvastatin IC <sub>50</sub> (μM)	95% Confidence interval (μM)
ZR-75-1	L108R/- (+/-)	2.56	2.376-2.76
Cama-1	D92H/- (+/-)	13.32	12.52-14.17
MCF7	+/+	20.17	18.38-22.15
T47D	+/+	24.66	19.36-31.05

TABLE 6 Coefficient of drug interaction (CDI) values of hydroxytamoxifen (OHT) and terbinafine (TBF) combinations in T47D TamR lines.

	OHT 2.5 μM + TBF 20 μM	OHT 2.5 μM + TBF 30 μM	OHT 5 μM + TBF 20 μM	OHT 5 μM + TBF 30 μM
T47D-TamR	0.95	0.75	0.43	0.35
T47D-TamR shPTEN	0.90	0.68	0.32	0.27

## 4 | DISCUSSION

PI3K pathway genes are frequently mutated in carcinogenesis, and PTEN loss of function is one of the common mutations. Complete loss of PTEN helps cells to overcome PIK3CA inhibition treatments via compensatory reactivation of p110β isoform.<sup>24</sup> Pan-PI3K inhibitors did not yield the expected clinical benefit due to a wide range of side effects mainly originating from liver toxicities. To overcome this situation, isoform-specific PI3K inhibitors were designed, but some studies suggest that treatments repressing the PI3K pathway transiently lead to generation of resistance. Cells become dependent predominantly the other PI3K isoform after inhibitor treatments, and the PI3K pathway is re-activate via feedback mechanisms through RTK.<sup>25</sup> In PTEN-loss-driven carcinogenesis, the mechanism that causes a change in isoform prevalence is not well understood.

The elucidation of the molecular processes governing this decision could improve the effective suppression of feedback responses, allowing the development of new combination therapeutics. In our study, metabolic rewiring mechanisms were investigated in PTEN loss- and activated PIK3CB-induced cancer models. Initially, we investigated potential drivers of PTEN loss-induced tumorigenesis in GEO datasets. Upon PI3K activation, a number of metabolic pathways were predominantly upregulated, and cholesterol biosynthesis emerged as an actionable module capable of pinpointing a potential metabolic vulnerability (Figure 1A). The cholesterol pathway is important for steroid hormone production, which is critical for hormone-dependent cancer types like breast, prostate, ovary, and so on. mRNA levels of SQLE, a rate-limiting enzyme in the synthesis of cholesterol, were significantly upregulated upon PI3K pathway activation in both PTEN depletion and expression of an activated p110β allele (Figure 1B,C). In silico analyses showed that the SQLE gene is highly altered in many cancer types and has a biomarker potential particularly for prostate and breast cancer (Figure 1D,E). A potential relationship between PI3K activity and the cholesterol production pathway was also investigated. The mRNA levels of cholesterol pathway genes increased with PTEN loss or excessive activation of the PI3K pathway upon expression of myristoylated p110β (Figure S1C,D). This trend might be reversed at the mRNA level in PTEN-null and hormone-independent PC3 cells with re-expression of PTEN (Figure 2A). Both in silico and qPCR results show that PI3K regulates the level of rate-limiting enzymes in the cholesterol synthesis pathway. Therefore, potential regulators of cholesterol synthesis might be the focus of prospective studies focusing on PTEN-loss-driven cancer types.

Our results further implicate that PTEN re-expression leads to a decrease in SQLE protein levels upon degradation in PC3, LNCaP,

and C4-2 cell lines (Figure 2B). According to previous studies, it is stated that SQLE regulates the PTEN status through epigenetic modifications.<sup>26</sup> Our findings further imply that the interaction between the PI3K pathway and SQLE can be bidirectional; activation of the pathway can modulate SQLE levels at both the transcriptional and post-translational levels. Furthermore, PTEN-null cell lines showed higher sensitivity to the cholesterol synthesis inhibitor terbinafine than PTEN-replete cells (Figure 3). These results are in agreement with our previous findings showcasing the sensitivity of PTEN-null hormone-dependent cancers to simvastatin.<sup>6</sup> Downstream molecules of PI3K, for example, S6 ribosomal protein Akt, have lower activation upon pharmacological inhibition in PTEN-null PC3s compared with PTEN-wt DU145s. The maintenance of lipid rafts, specifically with regards to sphingolipids and cholesterol is important for signal transduction and membrane trafficking. Signaling through the PI3K pathway is dependent on the integrity of lipid rafts. Limiting cholesterol production might lead to disruption of raft signaling in p110 $\beta$ -dependent PTEN-null cancer.<sup>6</sup> Furthermore, we have quantitatively shown that PTEN expression reduces the amount of cellular cholesteryl esters as well as free cholesterol in CRPC cells (Figure 4A,B). These findings corroborated previous reports depicting the importance of PTEN loss on accumulation of cholesterol esters.<sup>27</sup> However, our findings suggest that the observed buildup of cholesterol esters may be confirmed at the level of cellular free cholesterol and is accompanied by a rise in SQLE and, to a lesser extent, HMGCS levels. These results implicate a direct involvement of the PI3K pathway in cholesterol synthesis by regulating the levels of key enzymes in the pathway.

Our findings also imply that antihormone treatment might benefit from cotargeting of cholesterol synthesis in a variety of different experimental models of 2D, anchorage-independent, and spheroid growth, thereby improving the likelihood of tumor regression (Figure 5 and Figure S5). Analysis of breast cancer cells resistant to the antihormone agent tamoxifen revealed that these cells have elevated levels of SQLE (Figure 6A and Figure S6B). This provides a rationale for further research into antihormone treatment and cholesterol pathway synthesis inhibition in other hormone-dependent cancer subtypes. Finally, we discovered that SQLE has biomarker potential and that cancer cells' dependence on it may be modified by PTEN levels in tamoxifen-resistant T47D cells, opening up treatment options that combine the SQLE inhibitor terbinafine with the ER antagonist tamoxifen (Figure 6E,F and Figure S6C).

Overall, we showed that steroid hormone-dependent breast and prostate malignancies have a PTEN-dependent reliance on cholesterol metabolism. Also, p110 $\beta$  deregulation might promote an upregulation in the genes regulating cholesterol biosynthesis. Across all the key enzymes in the cholesterol pathway, SQLE might be a possible candidate of biomarker with theranostic potential for prostate and breast cancer (Figures S3 and S6). Our results demonstrated that PTEN-null cell lines have higher sensitivity for the inhibition of cholesterol synthesis. Upon biochemical analyses, SQLE protein levels were found to be decreased with PTEN reinduction in PTEN-null prostate cancer cell lines.

To overcome cancer recurrence, it is essential to develop sensible combinational therapy options. Components of the cholesterol synthesis pathway, such as SQLE, may be appealing for combinational therapies in PTEN-deficient, hormone-dependent cancers. Terbinafine is an antifungal treatment licensed by the FDA,<sup>28</sup> and drug repurposing might make it suitable for prospective PTEN-null cancer therapy. To validate the possibility of terbinafine in conjunction with antihormone treatment methods for extremely aggressive PTEN-null tumors, additional in vivo studies are warranted.

## ACKNOWLEDGMENTS

We thank Dr. Ozlem Aybuke Isik for critical reading of the manuscript.

## FUNDING INFORMATION

This project was supported by "Türkiye Bilimsel ve Teknolojik Araştırma Kurumu"; grant/award number: 118Z976.

## CONFLICT OF INTEREST STATEMENT

Ozgur Sahin is co-founder and manager of OncoCube Therapeutics LLC and is founder and president of LoxiGen, Inc. The other authors declare no conflict of interest.

## ETHICS STATEMENT

Approval of the research protocol by an Institutional Reviewer Board: N/A.

Informed consent: N/A.

Registry and the Registration No. of the study/trial: N/A.

Animal studies: N/A.

## ORCID

Onur Cizmecioglu  <https://orcid.org/0000-0002-7608-6950>

## REFERENCES

1. Jia S, Liu Z, Zhang S, et al. Essential roles of PI(3)K-p110beta in cell growth, metabolism and tumorigenesis. *Nature*. 2008;454(7205):776-779.
2. Horie Y, Suzuki A, Kataoka E, et al. Hepatocyte-specific Pten deficiency results in steatohepatitis and hepatocellular carcinomas. *J Clin Invest*. 2004;113(12):1774-1783.
3. Fang M, Shen Z, Huang S, et al. The ER UDPase ENTPD5 promotes protein N-glycosylation, the Warburg effect, and proliferation in the PTEN pathway. *Cell*. 2010;143(5):711-724.
4. Kalaany NY, Sabatini DM. Tumours with PI3K activation are resistant to dietary restriction. *Nature*. 2009;458(7239):725-731.
5. Garcia-Cao I, Song MS, Hobbs RM, et al. Systemic elevation of PTEN induces a tumor-suppressive metabolic state. *Cell*. 2012;149(1):49-62.
6. Cizmecioglu O, Ni J, Xie S, Zhao JJ, Roberts TM. Rac1-mediated membrane raft localization of PI3K/p110 $\beta$  is required for its activation by GPCRs or PTEN loss. *Elife*. 2016;5:e17635.
7. Llaverias G, Danilo C, Mercier I, et al. Role of cholesterol in the development and progression of breast cancer. *Am J Pathol*. 2011;178(1):402-412.
8. Cardwell CR, Hicks BM, Hughes C, Murray LJ. Statin use after diagnosis of breast cancer and survival: a population-based cohort study. *Epidemiology*. 2015;26(1):68-78.

9. Brown AJ, Chua NK, Yan N. The shape of human squalene epoxidase expands the arsenal against cancer. *Nat Commun*. 2019;10(1):888.
10. Mishra RR, Belder N, Ansari SA, et al. Reactivation of cAMP pathway by PDE4D inhibition represents a novel druggable axis for overcoming tamoxifen resistance in ER-positive breast cancer. *Clin Cancer Res*. 2018;24(8):1987-2001.
11. Timofeev O, Cizmecioglu O, Hu E, Orlik T, Hoffmann I. Human Cdc25A phosphatase has a non-redundant function in G2 phase by activating cyclin a-dependent kinases. *FEBS Lett*. 2009;583(4):841-847.
12. Demir M, Cizmecioglu O. ZAP70 activation compensates for loss of class IA PI3K isoforms through activation of the JAK-STAT3 pathway. *Cancer Diagn Progn*. 2022;2(3):391-404.
13. Huang DW, Sherman BT, Tan Q, et al. DAVID bioinformatics resources: expanded annotation database and novel algorithms to better extract biology from large gene lists. *Nucleic Acids Res*. 2007;35:W169-W175.
14. Huang DW, Sherman BT, Lempicki RA. Systematic and integrative analysis of large gene lists using DAVID bioinformatics resources. *Nat Protoc*. 2009;4(1):44-57.
15. Cerami E, Gao J, Dogrusoz U, et al. The cBio cancer genomics portal: an open platform for exploring multidimensional cancer genomics data. *Cancer Discov*. 2012;2(5):401-404.
16. Gao J, Aksoy BA, Dogrusoz U, et al. Integrative analysis of complex cancer genomics and clinical profiles using the cBioPortal. *Sci Signal*. 2013;6(269):p11.
17. Fekete JT, Györfy B. ROCplot.org: validating predictive biomarkers of chemotherapy/hormonal therapy/anti-HER2 therapy using transcriptomic data of 3,104 breast cancer patients. *Int J Cancer*. 2019;145(11):3140-3151.
18. Györfy B. Discovery and ranking of the most robust prognostic biomarkers in serous ovarian cancer. *GeroScience*. 2023;45(3):1889-1898.
19. Whale AD, Colman L, Lensun L, Rogers HL, Shuttleworth SJ. Functional characterization of a novel somatic oncogenic mutation of PIK3CB. *Signal Transduct Target Ther*. 2017;2:17063.
20. Moon H, Hill MM, Roberts MJ, Gardiner RA, Brown AJ. Statins: protectors or pretenders in prostate cancer? *Trends Endocrinol Metab*. 2014;25(4):188-196.
21. Fritsche-Guenther R, Gloaguen Y, Eisenberger A, Kirwan JA. Analysis of adherent cell culture lysates with low metabolite concentrations using the Biocrates AbsoluteIDQ p400 HR kit. *Sci Rep*. 2022;12(1):7933.
22. Gunti S, Hoke ATK, Vu KP, London NR. Organoid and spheroid tumor models: techniques and applications. *Cancers (Basel)*. 2021;13(4):1-18.
23. Sato R. Recent advances in regulating cholesterol and bile acid metabolism. *Biosci Biotechnol Biochem*. 2020;84(11):2185-2192.
24. Castel P, Toska E, Engelman JA, Scaltriti M. The present and future of PI3K inhibitors for cancer therapy. *Nat Cancer*. 2021;2(6):587.
25. Thorpe LM, Yuzugullu H, Zhao JJ. PI3K in cancer: divergent roles of isoforms, modes of activation, and therapeutic targeting. *Nat Rev Cancer*. 2015;15(1):7.
26. Liu D, Wong CC, Fu L, et al. Squalene epoxidase drives NAFLD-induced hepatocellular carcinoma and is a pharmaceutical target. *Sci Transl Med*. 2018;10(437):eaap9840.
27. Yue S, Li J, Lee SY, et al. Cholesteryl ester accumulation induced by PTEN loss and PI3K/AKT activation underlies human prostate cancer aggressiveness. *Cell Metab*. 2014;19(3):393-406.
28. Jensen JC. Clinical pharmacokinetics of terbinafine (Lamisil). *Clin Exp Dermatol*. 1989;14(2):110-113.

## SUPPORTING INFORMATION

Additional supporting information can be found online in the Supporting Information section at the end of this article.

**How to cite this article:** Kaysudu I, Gungul TB, Atici S, et al. Cholesterol biogenesis is a PTEN-dependent actionable node for the treatment of endocrine therapy-refractory cancers. *Cancer Sci*. 2023;00:1-11. doi:[10.1111/cas.15960](https://doi.org/10.1111/cas.15960)